Bifurcation Analysis of Various Power System Models

William D. Rosehart Claudio A. Cañizares
Department of Electrical and Computer Engineering
University of Waterloo
Waterloo, Ontario, Canada N2L 3G1

This paper presents the bifurcation analysis of a detailed power system model composed of an aggregated induction motor and impedance load supplied by an under-load tap-changer transformer and an equivalent generator and transmission system. Different modeling levels with their respective differential-algebraic equations are studied, to determine the minimum dynamic model of the system that captures the most relevant features needed for bifurcation studies of power systems. An aggregated model of a realistic load is used to illustrate the ideas presented throughout the paper.

Keywords: saddle-node and Hopf bifurcations, system modeling, voltage collapse.

I. Introduction

Voltage stability problems in power systems may occur for a variety of reasons, from voltage control problems with automatic voltage regulators (AVR) and under-load tap-changer (ULTC) transformers, to instabilities created by different types of bifurcations. Several conference proceedings[1-2] summarize most of the voltage stability problems, and discuss techniques and models proposed by several researchers relating to the area of bifurcation theory. These bifurcations are characterized by changes in the eigenvalues of the system equilibria as certain parameters change in the system. Typically, the generation or system loading levels are used as bifurcation parameters, which are varied slowly, moving the system from one equilibrium point to another. However, for certain values of the bifurcation parameters, more complicated behavior may result, leading to instability. Under these conditions it is possible for the system to exhibit oscillatory behavior[3], or even voltage collapse[4, 5]. These conditions are mathematically characterized by one of the system's eigenvalues becoming zero (saddle-node, transcritical, and pitchfork bifurcation), or by a pair of complex conjugate eigenvalues crossing the imaginary axis (Hopf bifurcation)[6].

The importance of system modeling in voltage stability studies, especially regarding the location of the bifurcation points and the corresponding system dynamic response, has been addressed in several studies[4, 7-8]. However, there has been little agreement in the power system community as to which particular models are adequate for these types of studies. Various models have been proposed[9-10] to capture the basic dynamic voltage response of the system.

In reference 11, the authors examine the characteristics of power systems where induction motors constitute a main portion of the load. In their study, three different induction motor load models are considered. The loads were modeled as constant, linear and quadratic functions of the induction motor rotor speed. Static loads were also included in the system model, allowing for the examination of the effect of changing the proportion of the total load which was composed of static elements. Fixed voltage, and constant power

generator models were used, with no generator dynamics considered. The study found that for constant load models, saddle-node bifurcations occurred at higher voltage levels and at higher speeds as compared to the speed dependent mechanical load models. Furthermore, in a simple example, the percentage of the total load composed of induction motor load did not affect the nature of bifurcations, but did influence the value of induction motor loading at which the bifurcations occurred.

In references 12 and 13, the effect of modeling dynamics of ULTC transformers on voltage stability is studied. The studies used a continuous time model of tap changers for the system transformers, arguing that such a model is an acceptable approximation of discrete tap movements in studies of voltage collapse. The focus of the studies were to determine control strategies to lock the transformers tap changers to help prevent voltage collapse when the system is heavily loaded based on the idea that voltage dependent loads require less reactive power support. The interaction between dynamics of under load tap changing transformers and loads were illustrated in this research, showing that such interaction plays a major role in bifurcations.

A Hopf bifurcations was detected, along with typical saddle-node bifurcations, in reference 8 with a simple two bus single generator system. The loads in the system were modeled using a third order induction motor model and lumped impedance elements. The system generator was modeled using a dynamic two-axis model with an IEEE type 1 exciter. Dynamic transmission line models were not incorporated into the studies. The use of dynamic transmission system models are presented in reference 7, with a simple single generator example.

In the current literature, individual components of power systems have been examined in bifurcation studies, but little attention has been placed on the possible interaction of different system components. This gap motivated the research presented in this paper. This paper examines the effect of using different levels of model detail on system bifurcations and their corresponding effect on voltage collapse phenomena. Different models of induction motors, ULTC transformers, dynamic transmission line models, and dynamic lumped load impedances are considered.

The paper is structured as follows. Section II briefly discusses the models used and some basic concepts of bifurcation theory are presented in Section III. In Section IV, bifurcation analyses are performed on a sample power system using several models, each incorporating different modeling details. Conclusions are presented in Section V.

II. System Models

A typical power system load[14] is used throughout the paper as a test system. This load is composed of 5 large induction motors of 5,600 HP (1, 3 and 4) and 1,600 HP (2 and 5), plus 5 distribution transformers and transmission lines. Each induction motor is assumed to have an additional impedance load connected at its terminals. The generator in bus 10 is used to model the power system feeding the load through an ULTC, to represent a typical supply scheme.

Using the techniques described in 15, the load may be aggregated to reduce the system to the model depicted in Figure 1, assuming a balanced three-phase system. The aggregated load is composed of a single induction motor and a static impedance load. The various steady state and dynamic models used to represent the different elements of this reduced system are described below.

II.1. Generator

The generator was modeled using both a simple Thevenin equivalent and a detailed dynamic model. For each of the models considered, the generator is used as the system reference. The detailed model of

the synchronous generator uses the standard set of p.u. $dq0$ equations for a rotor based reference frame connected to a balanced three-phase system[16], generally referred to as the flux model. The AVR is set to maintain a constant terminal voltage using a simple integrator control, i.e.,

$$\dot{v}_{fd} = \frac{1}{T_a}(V_{ref} - V_t) \tag{1}$$

where T_a is the time constant of the AVR, V_{ref} is a reference signal, and V_t is the magnitude of the generator terminal voltage.

No droop was introduced into the governor model to better match the steady state model of the generator, allowing for a better comparison of the different models of the system. Hence, the governor is simply modeled by

$$\dot{P}_m = \frac{1}{T_g}(\omega_{ref} - \omega_r) \tag{2}$$

where ω_{ref} is a reference speed, set to the desired output angular velocity, ω_r is the rotor speed, and T_g is the time constant of the governor. The mechanical power P_m and the mechanical torque T_m are related by:

$$P_m = \omega_r T_m \tag{3}$$

II.2. ULTC

The ULTC is assumed to be an ideal device, i.e., saturation and losses are neglected and any internal reactances is lumped into X_{th}. To simplify the analysis of the aggregated load while retaining some of the important voltage control features of the ULTC, this paper assumes a continuous control of V_2 with no limits. However, in practice, V_2 would typically be controlled discretely by the transformer taps within certain limits. The following equations were used to model the behavior of the ideal ULTC:

$$\begin{aligned} V_2 &= aV_1 \\ \dot{a} &= \frac{1}{T_t}(V_{2_0} - V_2) \end{aligned} \tag{4}$$

where a stands for the tap shift on the secondary side with respect to a nominal 1 p.u. value, V_{2_0} is the control set point, and T_t represents the ULTC time constant.

II.3. Transmission System

The transmission system of the supply network is modeled using an equivalent Thevenin impedance X_{th} in steady state. On the other hand, the dynamics of this transmission system could be described in a generalized dq reference frame as follows:

$$\begin{aligned}
\frac{d}{dt}i_q &= \frac{v_{1q} - v_{2q} - R_{ln}i_q - \psi_q/\omega}{L_s - L_m} \\
\frac{d}{dt}i_d &= \frac{v_{1d} - v_{2d} - R_{ln}i_d + \psi_d/\omega}{L_s - L_m} \\
\psi_q &= (L_s - L_m)i_q \\
\psi_d &= (L_s - L_m)i_d
\end{aligned} \tag{5}$$

where ω is the dq transformation reference frame speed, and $L_{ln} = L_s + L_m$. The zero-axis is not considered, as the system is assumed to be balanced.

II.4. Impedance Loads

The model used to describe the static system loads corresponds to the standard RL impedance model. When phasor models are used, the impedance load is modeled using the real and reactive demand of the load. Dynamics of the impedance load can be introduced by considering the differential equations used to describe the current through an inductor using a generalized dq reference frame as follows:

$$\begin{aligned}
\frac{d}{dt}i_{IL_q} &= \frac{v_q}{L_{IL}} - \omega i_{IL_d} \\
\frac{d}{dt}i_{IL_d} &= \frac{v_d}{L_{IL}} + \omega i_{IL_q}
\end{aligned} \tag{6}$$

where the d-axis and q-axis variables, d and q respectively, include the inductor current i_{IL} and the voltage at the load bus v. The resistive component of the impedance load is used to define the voltage v using the following linear algebraic equations:

$$\begin{aligned}
v_q &= R_{IL}(i_q - i_{IL_q}) \\
v_d &= R_{IL}(i_d - i_{IL_d})
\end{aligned} \tag{7}$$

II.5. Induction Motor Loads

The induction motor is modeled using the standard set of p.u. $dq0$ equations for a synchronously rotating reference frame connected to a balanced three-phase sinusoidal supply[17]. Reduced order models can be easily obtained from the standard model by eliminating certain derivative terms. For example, if the stator flux linkage transients are ignored, i.e., $\dot{\psi}_{qs} = \dot{\psi}_{ds} = 0$, the standard model is reduced to a third order model. By eliminating all differential terms, the induction motor is reduced to a simple steady state model represented by the impedances depicted in Figure 1 with a constant slip S.

The mechanical load torque T_l is simulated as a linear function of the rotor speed as follows:

$$T_l = \frac{\lambda}{\omega_e}\omega_r \tag{8}$$

where λ is used as a slow varying parameter to simulate changes in the mechanical load, ω_e is the synchronous reference frame speed, and ω_r is the rotor speed.

A requirement is that at equilibrium points the electro-magnetic torque T_e and the mechanical load T_l are of equal magnitude. Therefore, system equilibrium points occur at the intersection points of the torque-speed curves of both the induction motor and the mechanical load, as depicted in Figure 2. The number of intersections between the two curves represents the number of equilibrium points for a given value of λ; as λ varies the number of intersections between the curves changes. The value of λ for which the mechanical load intersects the maximum of the electro-magnetic torque curve represents the maximum loading of the system; this point is typically corresponds to the "knee" of the system power-voltage curve (PV curve). For loading values greater than the maximum loading, there will be little change in the speed and terminal voltage characteristics of the machine, since the intersection point of the two curves does not change significantly, yielding similar torque and speed (mechanical power) values for relatively large values of λ.

III. Bifurcation Theory

The scalar variable λ in (8) was chosen as the "loading" or "bifurcating" parameter, as changes to this parameter have an effect on the mechanical load of the system, which result in changes to the active and reactive power demands, with the corresponding effect on the load voltage; this is the typical situation encountered in voltage collapse studies. To carry out this analysis, the nonlinear equations of the system were linearized at each equilibrium point for the different system models. This linearized representation was then used to determine the stability of the equilibrium points by means of eigenvalue analysis. Of particular interest are the values of λ where the equilibrium points go from being stable to unstable, or from being unstable to stable, or when the number of these equilibrium points change. The operating points where these changes in stability occur are known as bifurcation points, and are typically characterized by system eigenvalues becoming zero (saddle-node, transcritical and pitchfork bifurcation), or by complex conjugate eigenvalue pairs crossing the imaginary axis (Hopf bifurcations).

The phenomena may be explained more rigorously by using the following vector representation:

$$\begin{aligned} \dot{x} &= f(x, y, \lambda) \\ 0 &= g(x, y, \lambda) \end{aligned} \tag{9}$$

Where, $x \in \Re^n$ is a vector of state variables, $y \in \Re^m$ is a vector of algebraic variables, and $\lambda \in \Re$ is any positive parameter in the system that changes slowly, moving the system from one stable equilibrium point to another until a bifurcation is encountered. The values of n and m change depending on the system model used. The scalar parameter λ in the sample system is defined as the load torque parameter in (8).

For the one-parameter dynamical system (9), non-singularity of the Jacobian $D_y g(\cdot)$ along system trajectories of interest, guarantees a well posed system[18] or strictly causal system[19, 20]. Thus, for this assumption, the following applies locally along these system trajectories:

$$\begin{aligned} & y = h(x, \lambda) \\ \Rightarrow \quad & \dot{x} = f(x, h(x, \lambda), \lambda) \\ & \quad = s(x, \lambda) \end{aligned} \tag{10}$$

If $D_y g(\cdot)$ becomes singular, then the model represented by (9) breaks down. When this occurs, some algebraic constraints could be transformed into differential equations to remove the singularity by changing the system models[21], or one may use singular perturbation to study the system[18]. (For a detailed analysis of the dynamic behavior of systems with singular $D_y g(\cdot)$ review reference 22.)

III.1. Saddle-Node Bifurcations

Saddle-node bifurcations are characterized by two equilibrium points of (9), typically one stable (s.e.p.) and one unstable (u.e.p.), merging at the bifurcation point (x_0, y_0) for the parameter value λ_0. This equilibrium point has a simple and unique zero eigenvalue of $D_x s|_0$ in (10), which corresponds to singularities of $D_{(x,y)}F|_0$, where $F(\cdot) = [f^T(\cdot)\ g^T(\cdot)]^T$ in (9)[21]. If the two merging equilibria coexist for $\lambda < \lambda_0$, then the two equilibrium points locally disappear when $\lambda > \lambda_0$, or vice versa[6, 23].

III.2. Hopf Bifurcations

Hopf bifurcations do not yield any changes in the number of equilibrium points. These types of bifurcations are characterized by a complex conjugate pair of eigenvalues for the equilibrium point (x_0, y_0, λ_0) of (9) lying on the imaginary axis of the complex plain. When the parameter λ changes, the complex conjugate pair moves away from the imaginary axis, either to the right or to the left of the axis. In this case, stable or unstable limit cycles (system oscillations) appear or disappear. Depending on the stability of these limit cycles and where they occur with respect to the bifurcation value parameter value λ_0, the Hopfs can be either subcritical or supercritical[6, 23].

III.3. Detection Methods

Direct and continuation methods can be used to detect bifurcations[6]. Direct methods have been successfully applied to determine the exact location of saddle-nodes in power systems[24]; however, these methods present serious numerical difficulties when used to locate Hopf bifurcations in differential-algebraic models of the type represented by (9)[25]. Continuation methods, on the other hand, can be used in all cases to detect any type of bifurcation without major difficulties[24, 25].

In this paper, a combination of both methods were used to determine the location and type of bifurcations in the test system. Several software packages were used to obtain the results depicted in the next section. Of these packages, AUTO97 [26] was particularly useful to determine locations and types of bifurcations, especially in the case of Hopf bifurcations where determining stability of limit cycles may be a rather difficult numerical problem[25].

IV. Results

The objectives of the analysis are focused on modeling issues in bifurcation analysis. Comparisons of the results of the different models can determine the appropriate level of modeling required to capture the most relevant features needed for bifurcation analysis; this is especially useful for voltage collapse studies. Because of the nature of a power system, different components and parts of individual components have different dynamical responses. The time constant associated with the components and their interactions influence the formation of bifurcations. By comparing different models of the induction motor load and the system, one may determine the levels of modeling required for these types of studies.

The idea is to remove all nonlinear algebraic constraints from the model, thereby eliminating the possibility of these constraints becoming singular[22].

IV.1. Detailed Induction Motor and ULTC Model

The bifurcation analysis was first performed on the system with only the induction motor and the ULTC transformer modeled with differential equations. The transmission line, impedance load, and the generator

are modeled with strictly algebraic equations.

The equivalent generator was modeled with a simple Thevenin circuit, to gain insight into the load behavior without complex generator models. The real and reactive power being injected at the ideal ULTC from the Thevenin source is equal to the real and reactive demand of the load, i.e.,

$$\begin{aligned} P &= V_2^2 G + P_{IM} \\ Q &= V_2^2 B + Q_{IM} \end{aligned} \tag{11}$$

where P_{IM} and Q_{IM} represent the real and reactive powers absorbed by the machine component of the load, and $V_2^2 G$ and $V_2^2 B$ represent the real and reactive powers absorbed by the static impedance component of the load.

The static generator and induction motor equations together with equations (4), (8) and (11) were simulated in AUTO97 in order to detect bifurcations for the test system depicted in Figure 1, for the parameter values given in Table 1. Using the methods described above, bifurcations diagrams for the fifth, third and first order induction motor models were obtained.

Figures 3 through 6 depict the equilibrium points (stable and unstable) and bifurcations for the fifth order induction motor model. The load varies with changes in the mechanical torque parameter λ. Figure 3 shows two saddle-node bifurcations at $\lambda_{SN_1} = 0.572672$ and $\lambda_{SN_2} = 0.281250$, and a subcritical Hopf bifurcation at $\lambda_{HB} = 0.569044$ of an approximate period of 12.6 seconds. Observe that for relatively large values of λ, the voltage does not change significantly due to little change on the power demand of the motor, as previously explained using Figure 2. The subcritical Hopf occurs just before the first saddle-node in the loading process; this behavior has been reported for other system models[21, 25] as well. The limit cycles associated with the Hopf bifurcation are depicted in Figure 4. A change of stability of these limit cycles is also shown in this Figure which might hint to the possible onset of chaotic motion. However, it was not numerically possible to determine the nature of this change.

Figure 5 shows the total load power P versus input voltage V_1 for the system, i.e., the system PV curve, which is a typical study tool used in voltage collapse analysis of power systems. Observe that the Hopf bifurcation (HB) occurs before the nose of the curve or maximum loading point, as shown in Figure 6. Furthermore, this maximum loading point does not correspond exactly to the first saddle-node bifurcation (SN1); these two points generally coincide when simplified load models are used[5]. The limit cycles associated with the subcritical Hopf are also depicted in the PV curve of Figure 6. The second saddle-node bifurcation (SN2) indicates that stable equilibrium points exist on the lower portion of the curve; this bifurcation is of no practical interest due to the rather low system voltages. Analysis of induction motor operation on the lower side of the PV curve has been investigated in reference 27.

Tests with several motor models and various parameter values were also carried out to determine their effect on the bifurcation points. For the first and third order models of the induction motor, only the two saddle-node bifurcations were detected. In order to determine the effect of the interaction between the induction motor and the ULTC, the model was modified so that it was composed of only the induction motor, supplied from an equivalent voltage source; in this case, only the two saddle-node bifurcations were detected. The values of the different impedances used to represent the static load $G + jB$ and the Thevenin impedance X_{th} were varied, observing that the presence and location of the Hopf bifurcation was a function of the value of X_{th}, and to a lesser extent, G and B. Reducing or increasing the value of X_{th} eliminated the Hopf; a Hopf bifurcation first appears at $X_{th} = 0.074$ for which the distance between the Hopf and the first saddle-node is the greatest. This Hopf moves toward the saddle-node as X_{th} increases and disappears again at $X_{th} = 0.6$. Although changing G and B have similar effects on the Hopf bifurcation, larger value changes are required to obtain similar results as when changing X_{th}.

Due to the algebraic equations introduced by the impedance load, transmission system and generator,

some numerical difficulties arose in the implementation of the system. When using the fifth order induction motor, a closed form expressions describing the system was found using the software package MAPLE [28]. For the first and third order induction motor models, no closed form expression for the algebraic variables could be determined due to their nonlinear complexity; in this case AUTO97 could not be used for the studies, and hence MATLAB [29] routines were developed and used.

IV.2. Detailed Transmission Line and Load Model

The system considered in Section IV.1 was extended to model the impedance load and the transmission system using differential equations. This allowed for the examination of the interaction of the transmission system and the fifth order induction motor model, and eliminated nonlinear algebraic constraints associated with the transmission line as their time constants are considered similar. The d-axis and q-axis inductances for the transmission line and impedance load were selected to match the steady-state parameters given in Table 1.

The static generator, induction motor equations and equations (4), (5) and (8) were then simulated in AUTO97 and MATLAB in order to detect bifurcations for the system of Figure 1 and Table 1. The generator q and d axis voltages in (5) were set to 1 and zero respectively to match the original model. From the simulations, bifurcations diagrams were obtained. In this analysis, only the fifth order induction motor model was used and the ULTC transformer was not removed from the model. Reduced order load models were not considered, since the motivation to include detailed transmission system models was to investigate their appropriateness when examining bifurcations due to induction motors loads; by reducing the order of the induction motor model, the interaction between the transmission system and the induction motor would be effectively removed.

Figures 7 depicts the eigenvalues for the range of loading considered in Section IV.1. This figure shows only the eigenvalues positioned close to the imaginary axis. There is a pair of purely complex eigenvalues fixed on the imaginary axis; the magnitude of these two eigenvalues, i.e., 377, corresponds to the fundamental frequency. The absolute value of the eigenvectors associated with these two imaginary eigenvalues at the initial system loading are shown in Table 2. The eigenvectors clearly indicates that the two eigenvalues fixed on the imaginary axis are largely a function of the transmission line d and q-axis current. To move these pair of eigenvalues away from the imaginary axis, a very small line resistance R_{ln} was incorporated into the model, so that it does not have an effect on the original system bifurcations. As discussed later, this indicates that the use of lossless transmission line models, when modeling the transmission system with algebraic equations, is acceptable to reduce complexity, but should not be used with more detailed models.

Figure 8 depicts the equilibrium points (stable and unstable) and bifurcations for the system, as the load varies with changes in the mechanical torque parameter λ. Two saddle-node bifurcations at $\lambda_{SN_1} = 0.572672$ and $\lambda_{SN_2} = 0.281250$ are depicted, together with a subcritical Hopf bifurcation at $\lambda_{HB} = 5.567003$ of an approximate period of 8.2 seconds. The presence of Hopf bifurcation is clearly illustrated in Figure 9 with an enlargement of the eigenvalues of Figure 7 focussed at the origin.

The use of differential equations to model the transmission system and impedance load created numerical problems with AUTO97. Due to the size of the problem, the program could not properly analyze the limit cycles associated with the Hopf bifurcation.

IV.3. Detailed System Model

The final analysis incorporated a detailed model for the entire system, including the synchronous generator. Due to the nature of the machine model, the composition of the generator terminal voltage is different

than the other model. In the first two models, the d-axis voltage was set to zero and the q-axis voltage was set to unity. Using the detailed generator model, this is not possible, as the d-axis voltage is a function of the d-axis current. Although the total voltage magnitude was fundamentally composed of the q-axis voltage, the difference in the models should be noted.

The detailed flux generator and induction motor equations together with equations (1) to (8) were simulated in MATLAB in order to obtain the bifurcation diagrams for the test system of Figure 1 and Tables 1 and 3.

Figure 10 depicts the equilibrium points (stable and unstable) and bifurcations for the complete system model, as the load varies with changes in the mechanical torque parameter λ. Two saddle-node bifurcations at $\lambda_{SN_1} = 0.572660$ and $\lambda_{SN_2} = 0.281250$ are present in the system, with a Hopf bifurcation at $\lambda_{HB} = 0.555149$. Again, the Hopf bifurcation occurs just before the first saddle-node in the loading process.

Because of the number of states in the complete model, AUTO97 was not able to perform the continuation analyses. MATLAB was used to determine initial starting points with over six digits of accuracy but, AUTO97 still was not able to converge; therefore, MATLAB routines where used to calculate the equilibrium points and eigenvalues.

IV.4. Comparison of Results

In this paper, several models for the same power system were used. The most detailed system model included a complete description of the system from the generator to the load. The least detailed model used a first order induction motor model and several nonlinear algebraic equations for modeling the transmission system and the supply source. For each model, parameters where determined such that the models had equal steady state values for equivalent loading levels. A minor exception to this occurred with the voltages of the detailed generator model, described in Section IV.3, because of the nature of the synchronous machine model, as compared to a Thevenin equivalent.

Table 4 illustrates the bifurcations that were encountered for the different models. For the first and third order models of the induction motor, only the two saddle-node bifurcations were detected. When the ULTC transformer was removed from the model, again only the two saddle-node bifurcations were detected. Observe that the value of the initial period decreased when more detailed systems where used. The results indicate that the first order model is an acceptable approximation to the full aggregated induction motor dynamics, when the the objective of the analysis is mostly interested in the location of saddle-node or other singular bifurcations[30]. For analysis of higher order dynamics, such as Hopf bifurcations, more detailed models are required, which is expected from previous results[21, 25].

The *Detailed Induction Motor and ULTC Model* section of Table 4 indicate that system components, such as the ULTC transformer, play a critical role in the occurrence of Hopf bifurcations and indicates that some elements in a power system cannot be evaluated independently, as their interaction may significantly affect the dynamic response. But the remaining sections, showing results when detailed models of the transmission system and generator have been included, indicate these component do no have a large effect on the occurrence of bifurcations in this case; the detailed models do have a minor effect on the location of the bifurcations. Analysis of the eigenvectors associated to the Hopf bifurcations were inconclusive with regards to pointing to a dominate parameter responsible for the bifurcation. This suggests that the need to model transmission systems using differential equations in bifurcations studies may not be required for the detection of bifurcations. Although more studies might be required, the results strongly suggest that the dynamics of impedance loads and transmission lines do not have a major effect on bifurcations associated with inductor motor loads and generator sources.

V. Conclusions

This paper presents a complete bifurcation study of different order models of aggregated induction motors fed by ULTC transformers. First order models of induction motors are shown to be adequate for saddle-node bifurcation studies, whereas steady state models are proven to be inadequate for these types of analyses. Thus, the paper clearly shows that at least the mechanical dynamics of aggregated loads should be included in voltage collapse studies of power systems, so that reasonable results can be obtained. When oscillatory modes associated with Hopf bifurcations are of interest, high order models must be used.

When the aim of bifurcation studies are to examine the existence of limit cycles, which are associated with Hopf bifurcations, detailed generator, ULTC transformer and induction motor models should be used. But it is not required to consider detailed dynamic transmission line models. Considering detailed transmission models may be advantageous in reducing computational complexity due to algebraic constraints.

VI. References

1 **Fink, L. H, editor** *Proc. Bulk Power System Voltage Phenomena II—Voltage Stability and Security* ECC Inc., Fairfax, VA (August 1991)

2 **Fink, L. H, editor** *Proc. Bulk Power System Voltage Phenomena III—Voltage Stability and Security* ECC Inc., Fairfax, VA (August 1994)

3 **Ajjarapu, V and Lee, B** 'Bifurcation theory and its application to nonlinear dynamical phenomena in an electrical power system' *IEEE Trans. Power Systems* Vol 7 No 2 (February 1992) pp 424–431

4 **Cañizares, C. A** 'On bifurcations, voltage collapse and load modeling' *IEEE Trans. Power Systems* Vol 10 No 1 (February 1995) pp 512–522

5 **Cañizares, C. A and Rosehart, W. D** 'Bifurcation analysis of induction motor loads for voltage collapse studies' *Proc. NAPS* M.I.T. Cambridge, Massachusetts (November 1996) pp 559–565

6 **Seydel, R** *From Equilibrium to Chaos—Practical Bifurcation and Stability Analysis* Elsevier Science North-Holland (1988)

7 **Lesieutre, B. C, Sauer, P. W and Pai, M. A** 'Transient algebraic circuits for power system dynamic modelling' *Electrical power and Energy Systems* (October 1993) pp 315–321

8 **Pai, M. A, Sauer, P. W and Lesieutre, B. C** 'Static and dynamic nonlinear loads and structural stability in power systems' *Proceedings of the IEEE* (November 1995) pp 1562–1572

9 **Xu, W and Mansour, Y** 'Voltage stability analysis using generic dynamic load models' *IEEE Trans. Power Systems* Vol 9 No 1 (1994) pp 479–493

10 **Sauer, P. W, Lesieutre, B. C and Pai, M. A** 'Dynamic vs. static aspects of voltage problems' pp. 207–216 in 1

11 **Popovic, D, Hiskens, I and Hill, D. J** 'Stability analysis of induction motor networks' Technical Report University of Sydney Sydney, NSW 2006, Australia

12 **Popovic, D, Hiskens, I, Makarov, Y and Hill, D. J** 'Tap locking strategies for emergency voltage control in power supply systems' *Proceedings of the 12th Power Systems Computation Conference, Dresden Germany* Vol 1 (August 1996) pp 309–315

13 **Popovic, D, Hiskens, I, Makarov, Y and Hill, D. J** 'Investigation of load-tap changer iteraction' *Electrical Power and Energy Systems* Vol 18 No 2 (1996) pp 81–97

14 **Lem, T. Y. J and Alden, R. T. H** 'Comparison of experimental and aggregated induction motor responses' *IEEE/PES 94 WM 168-5 PWRS, New York, NY* (November 1994) pp 1895–1900

15 **DiManno, J, Rogers, G. J and Alden, R. T. H** 'An aggregated induction motor model for industrial plants' *IEEE Trans. Power Apparatus and Systems* Vol 103 No 4 (April 1984) pp 683–690

16 **Kundur, P** *Power Systen Stability and Control* McGraw Hill Publishing Company New York (1994)

17 **Krause, P. C, Wasynckuz, O and Sudhoff, S. D** *Analysis of Electric Machinery* IEEE Press New York (1995)

18 **DeMarco, C. L and Bergen, A. R** 'Application of singular perturbation techniques to power system transient stability analysis' *Proc. ISCAS* (May 1984) pp 597–601

19 **Kwatny, H. G, Pasrija, A. K and Bahar, L. Y** 'Static bifurcations in electric power networks: Loss of steady-state stability and voltage collapse' *IEEE Trans. Circuits and Systems* Vol 33 No 10 (October 1986) pp 981–991

20 **Guo, T and Schlueter, R. A** 'Identification of generic bifurcation and stability problems in power system differential-algebraic model' *IEEE. Trans. Power Systems* (May 1994) pp 1032–1044

21 **Cañizares, C. A** 'Conditions for saddle-node bifurcations in ac/dc power systems' *Int. J. of Electric Power & Energy Systems* Vol 17 No 1 (February 1995) pp 61–68

22 **Venkatasubramanian, V, Schättler, H and Zaborszky, J** 'A taxonomy of the dynamics of the large power systems with emphasis on its voltage stability' pp. 9–52 in 1

23 **Guckenheimer, J and Holmes, P** *Nonlinear Oscillations, Dynamical Systems, and Bifurcations of Vector Fields* Springer-Verlag New York (1986)

24 **Cañizares, C. A and Alvarado, F. L** 'Point of collapse and continuation methods for large ac/dc systems' *IEEE Trans. Power Systems* Vol 8 No 1 (February 1993) pp 1–8

25 **Cañizares, C. A and Hranilovic, S** 'Transcritical and Hopf bifurcations in ac/dc systems' pp. 105–114 in 2

26 **Doedel, E, Wang, X, Champneys, A, Fairgrieve, T, Sandstede, B, Kuznetsov, Y and Fairgrieve, T** 'Auto97 continuation and bifurcation software for ordinay differential equations' Technical Report California Institute of Technology Pasadena, CA 91125 (1997)

27 **Gustafsson, M. N, Krantz, N. U and Daalder, J. E** 'Voltage stability: the significance of induction motor loads' *Proc. NAPS* Bozeman, Montana (October 1995) pp 394–402

28 **Char, B. W et al** *Maple V Language Reference Manual* Springer-Verlag (1991)

29 The Math Works Inc. Natick, Massachusetts *MATLAB* (1993)

30 **Dobson, I** 'The irrelevance of load dynamics for the loading margin to voltage collapse and its sensitivities' pp. 509–518 in 2

William D. Rosehart was born in Thunder Bay, Ontario, Canada, in 1972 He received his Bachelor's Degree in Applied Science, Electrical Engineering in 1996 and a Master's Degree in Applied Science in 1997 from the University of Waterloo. From 1991 to 1995 through the cooperative education program at the University of Waterloo, he worked in the Power Industry in Canada, including the Large Motors Division of GE Canada, Hammond Manufacturing, and Waterloo North Hydro. He is currently studying for his PhD degree at the University of Waterloo.

Claudio A. Cañizares was born in Mexico, D.F. in 1960. In April 1984, he received the Electrical Engineer diploma from the Escuela Politécnica Nacional (EPN), Quito-Ecuador, where he was a Professor for several years. His MS (1988) and PhD (1991) degrees in Electrical Engineering are from the University of Wisconsin–Madison. Dr. Cañizares is currently an Associate Professor at the University of Waterloo, Department of Electrical & Computer Engineering, and his research activities are mostly concentrated in the study of stability issues in power systems.

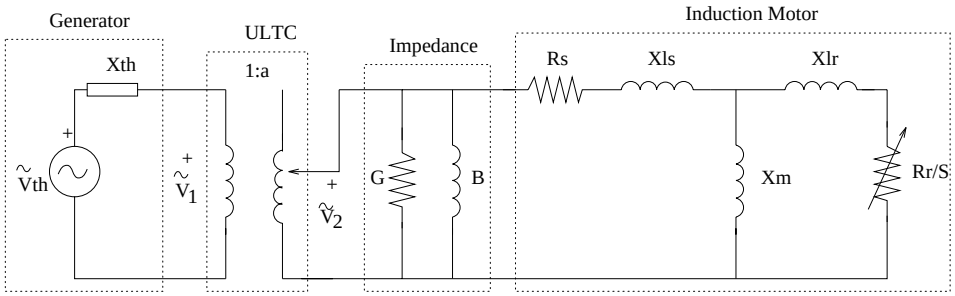

Figure 1: Aggregated load model of the test system. The source is modeled with a simple Thevenin equivalent to represent the supply power system.

Table 1: Aggregated Load Data (100MVA, 4KV Base)

Variable	Value (p.u.)
R_s	0.07825
X_{ls}	0.8320
X_m	16.48
R_r	0.1055
X_{lr}	0.8320
H	0.1836 s
ω_e	$2\pi 60$ s^{-1}
G	0.06047
B	0.03530
X_{th}	0.2
T_t	5 s
V_{2_0}	1

Table 2: Eigenvectors for System at Initial Loading Conditions

Parameter	EV-1 Magnitude
ψ_{qs}	1.6228e-10
ψ_{ds}	1.6317e-10
ψ_{qr}	1.0149e-11
ψ_{dr}	1.0093e-11
ω_r	3.5110e-10
i_{IL_q}	4.9057e-01
i_{IL_d}	4.9057e-01
i_q	5.0926e-01
i_d	5.0926e-01
a	2.4972e-14

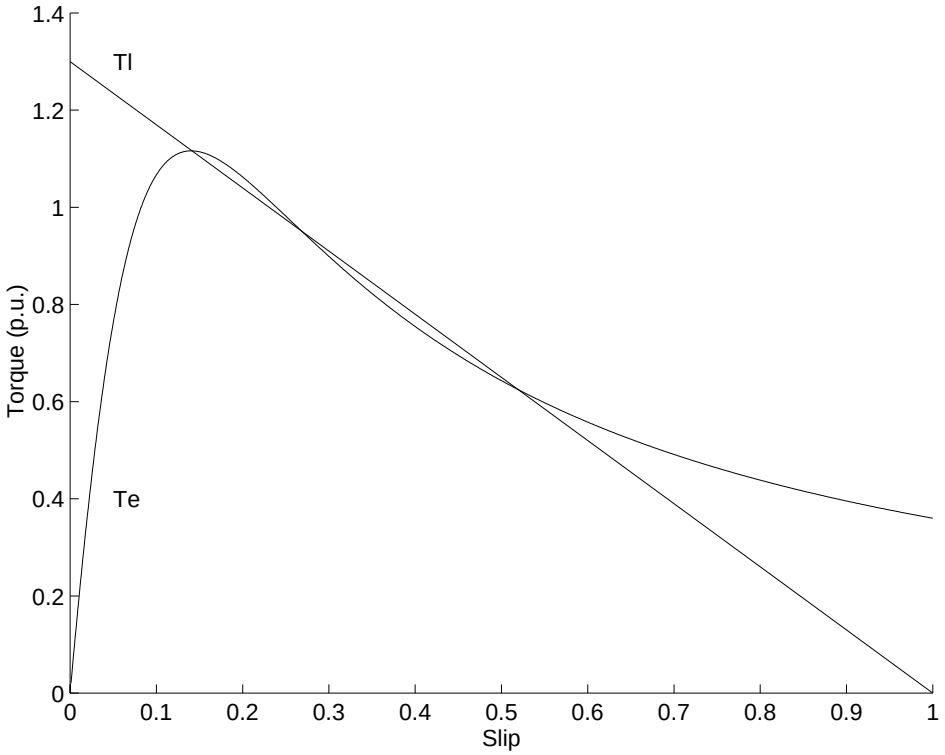

Figure 2: Steady state torque characteristics of the induction motor and mechanical load, for $\lambda = 1.3$.

Table 3: Synchronous Generator Parameters

Variables	Value
T_a	2.0000 s
H	2.3700 s
T_g	1.0000 s
ω_e	377 rad/s
R_s	0.000100
R_{kq2}	0.054000
R_{fd}	0.000742
R_{kd}	0.001096
X_{ls}	0.090000
X_{fd}	0.015000
X_{kd}	1.605000
X_{kq2}	1.526000
X_q	1.6400
X_d	1.7000
X_{mq}	0.028378
X_{md}	0.028378

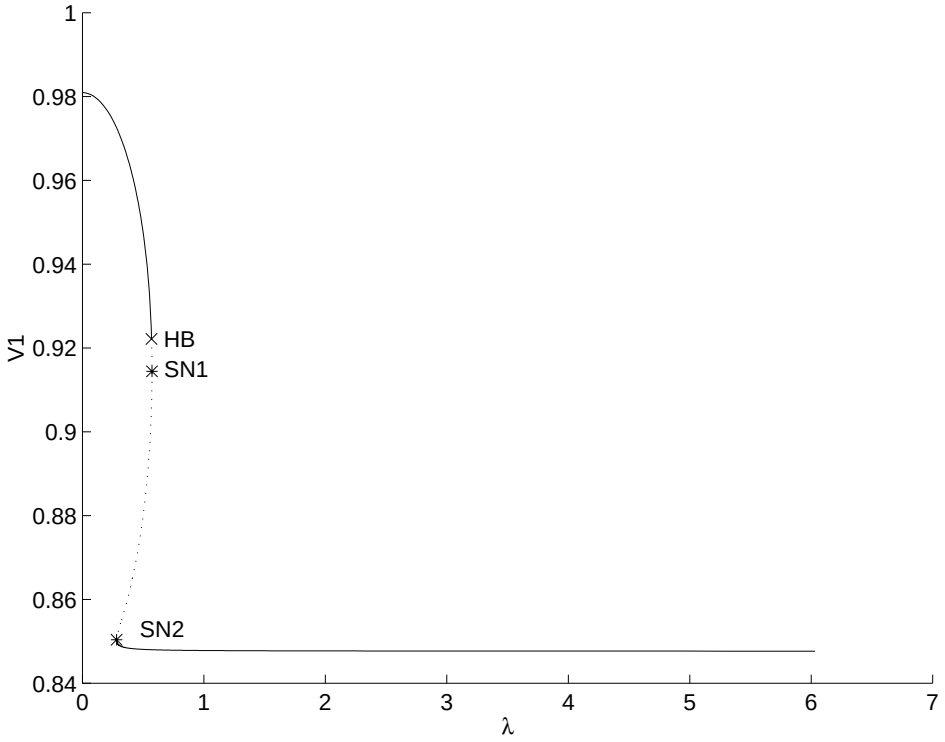

Figure 3: Bifurcations diagram of V_1 for fifth order model. The s.e.p.s are represented with a continuous line, whereas the u.e.p.s are depicted with a dotted line.

Table 4: Eigenvalues for Saddle Node (SN) and Hopf Bifurcations (HB) for Different Models

System Model	SN_1	SN_2	HB
Detailed Induction Motor and ULTC Model (Sec. IV.1.)			
• Fifth Order Motor Model with ULTC	0.572672	0.281250	0.569044
• Fifth Order Motor Model without ULTC	0.512377	0.228047	No Hopf
• Third Order Motor Model with ULTC	0.572672	0.281250	No Hopf
• First Order Motor Model with ULTC	0.572672	0.281250	No Hopf
Detailed Transmission Line and Load Model (Sec. IV.2.)	0.572672	0.281250	0.5567003
Detailed System Model (Sec. IV.3.)	0.572660	0.281250	0.555149

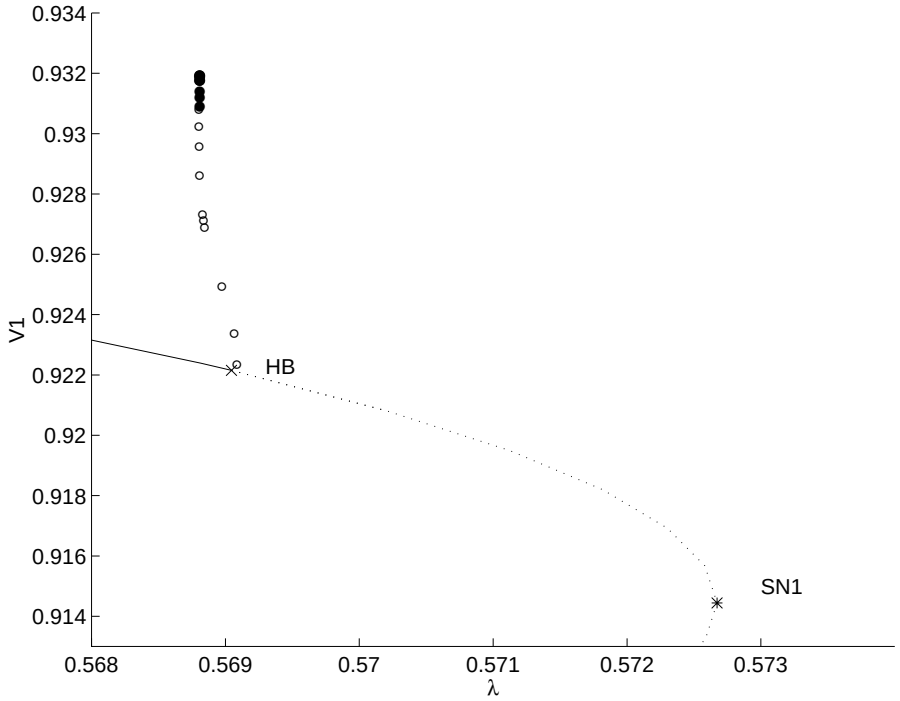

Figure 4: Enlargement of the bifurcations diagram of Figure 3. Stable and unstable limit cycles are depicted using black and clear circles, respectively.

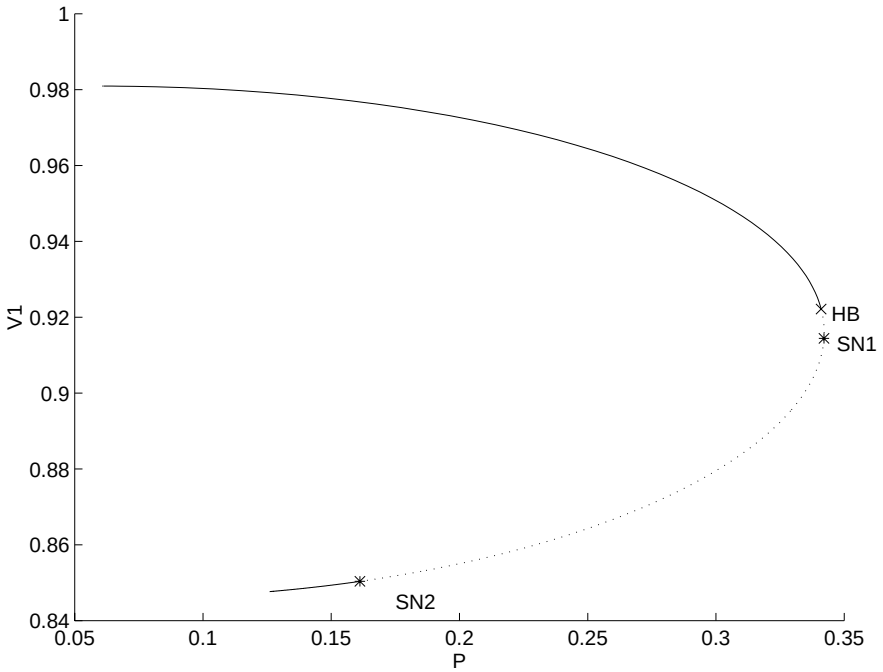

Figure 5: PV curve of V_1 for fifth order model. The s.e.p. are represented with a continuous line, whereas the u.e.p. are depicted with a dotted line.

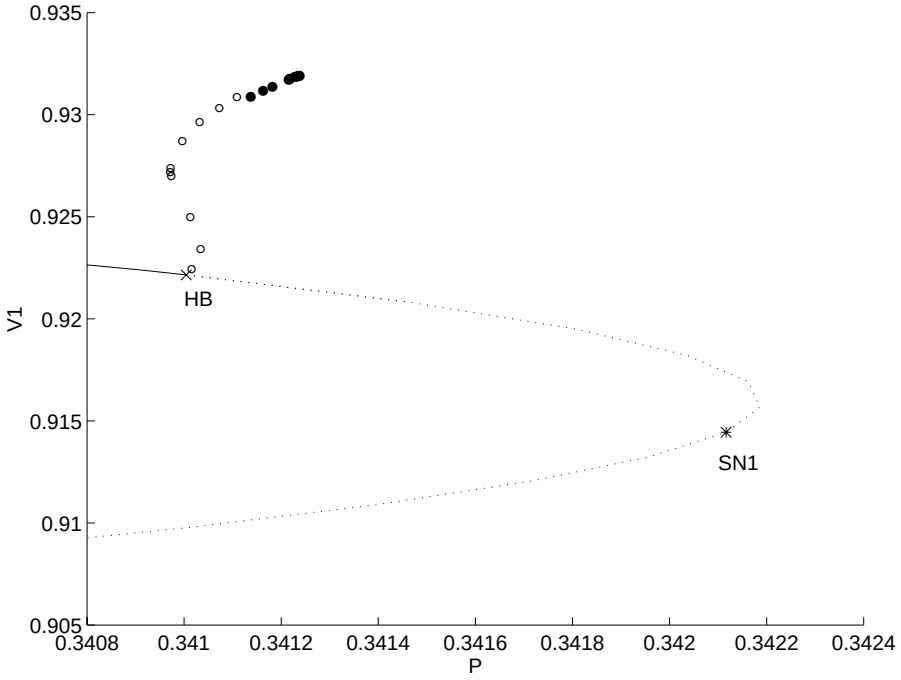

Figure 6: Enlargement of PV curve of Figure 5. Stable and unstable limit cycles are depicted using black and clear circles, respectively.

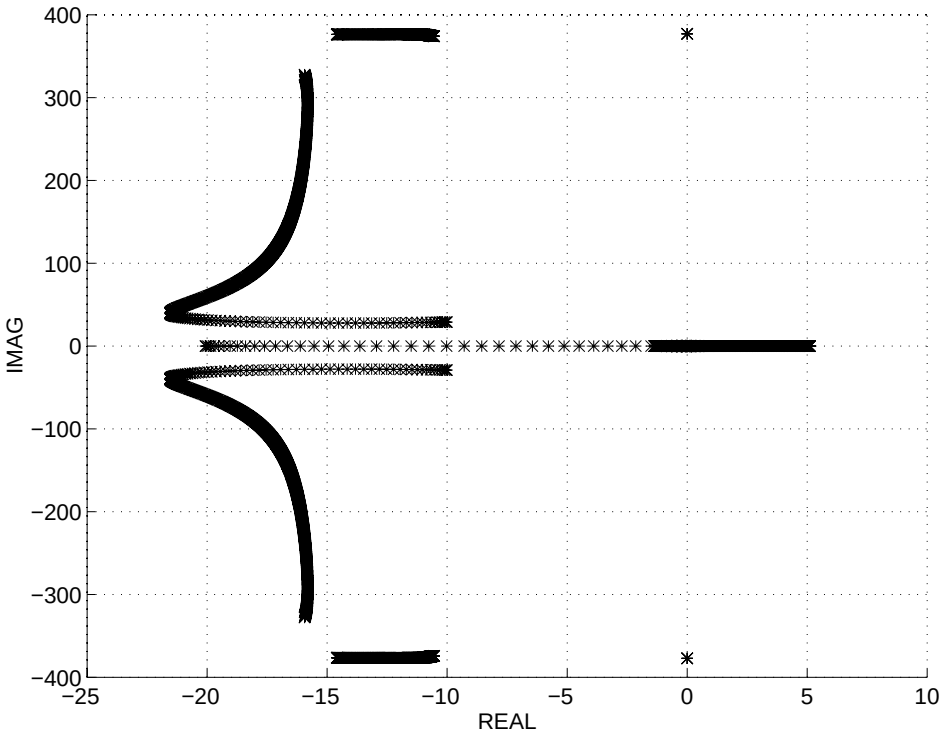

Figure 7: Eigenvalues of Detailed Transmission Line and Load Model

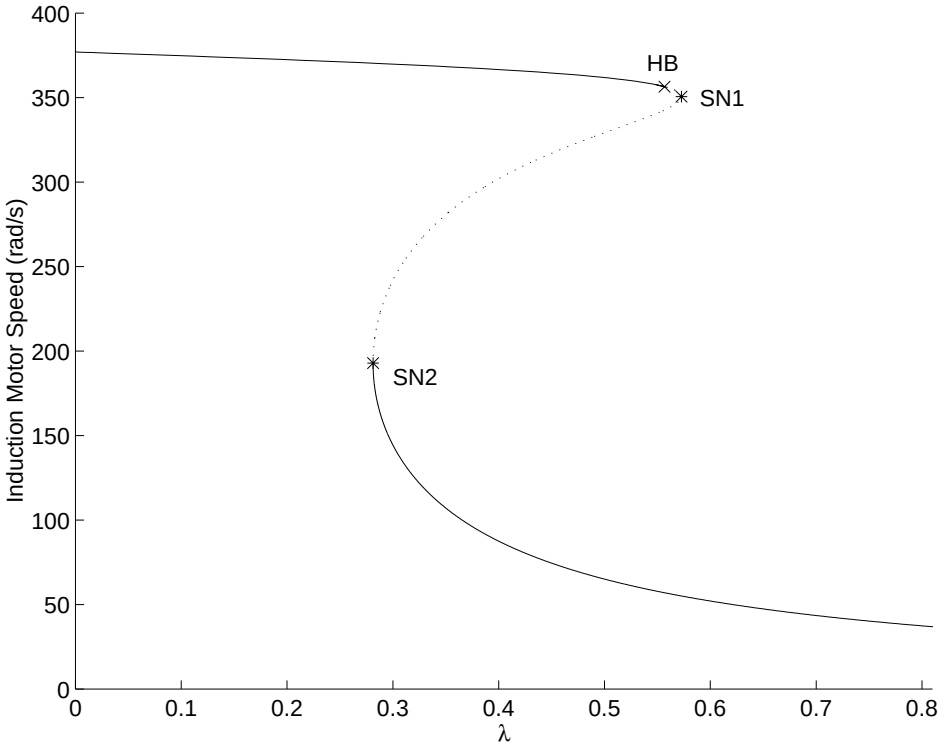

Figure 8: Bifurcation diagram of induction motor speed vs ω_r.

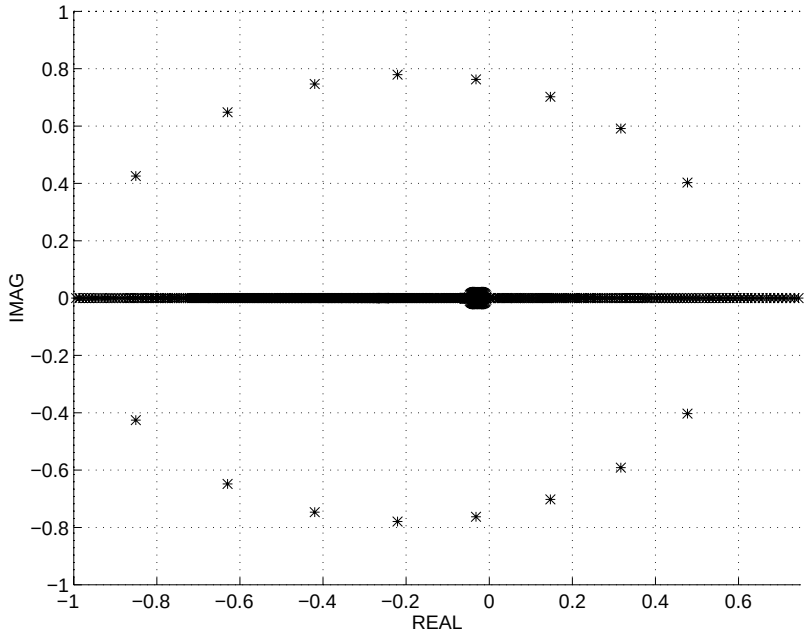

Figure 9: Enlargement of the eigenvalue diagram of Figure 7.

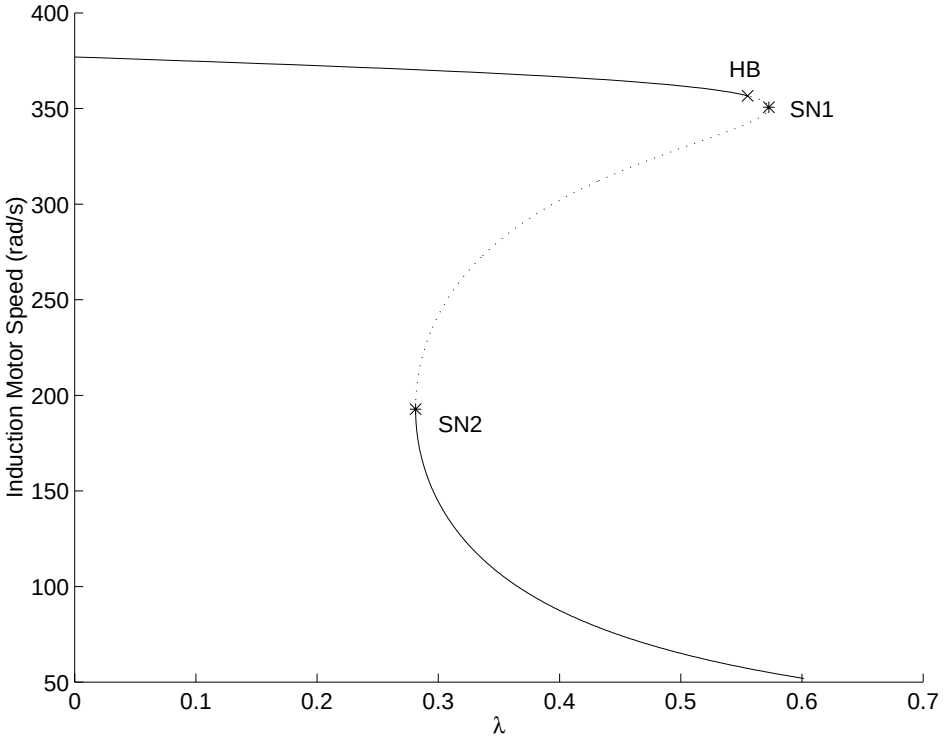

Figure 10: Bifurcations diagram of ω_r for complete system model. The s.e.p.s are represented with a continuous line, whereas the u.e.p.s are depicted with a dotted line.